Czech Technical University in Prague

Faculty of Electrical Engineering

BACHELOR THESIS

Yehor Zhyliaiev

Driving envelope protection using hierarchical control structure

Department of Control Engineering

Supervisor of the bachelor thesis: Ing. Denis Efremov

Study programme: Cybernetics and Robotics

Prague 2020

BACHELOR'S THESIS ASSIGNMENT

I. Personal and study details

Student's name: **Zhyliaiev Yehor** Personal ID number: **465814**

Faculty / Institute: **Faculty of Electrical Engineering**

Department / Institute: **Department of Control Engineering**

Study program: **Cybernetics and Robotics**

II. Bachelor's thesis details

Bachelor's thesis title in English:

Driving envelope protection using hierarchical control structure

Bachelor's thesis title in Czech:

Vývoj řídicích systémů pro ochranu jízdní obálky pomocí hierarchického přístupu

Guidelines:

The goal of the thesis is to investigate driving envelope definition and suggest possible control architecture to protect its restrictions. Provide validation and verification on a car simulator.
1) Study driving envelope definition and interpret it from physical point of view.
2) Adopt single-track model for design purposes.
3) Suggest suitable hierarchical control approach(-es) to protect boundaries defined by the driving envelope.
4) Provide validation and verification ride test using racing simulator "Life for Speed".
5) Provide comparison of the controlled vehicle (with envelope protection algorithm) and driven vehicle by human.

Bibliography / sources:

[1] Schramm, D., Hiller, M., & Bardini, R. (2014). Vehicle dynamics. Modeling and Simulation. Berlin, Heidelberg,151.
[2] Franklin, G. F., Powell, J. D., Emami-Naeini, A., & Powell, J. D. (1994). Feedback control of dynamic systems (Vol. 3). Reading, MA: Addison-Wesley.
[3] Efremov, D., Klaučo, M., Haniš, T., & Hromčík, M. (2019) "Driving envelope definition and envelope protection using model predictive control". Submitted on American Control Conference (ACC2020).
[4] Pratt, R. W. (Ed.). (2000). Flight control systems. American Institute of Aeronautics and Astronautics.

Name and workplace of bachelor's thesis supervisor:

Ing. Denis Efremov, Department of Control Engineering, FEE

Name and workplace of second bachelor's thesis supervisor or consultant:

Ing. Tomáš Haniš, Ph.D., Department of Control Engineering, FEE

Date of bachelor's thesis assignment: **10.01.2020** Deadline for bachelor thesis submission: **22.05.2020**

Assignment valid until:
by the end of summer semester 2020/2021

Ing. Denis Efremov Supervisor's signature	prof. Ing. Michael Šebek, DrSc. Head of department's signature	prof. Mgr. Petr Páta, Ph.D. Dean's signature

III. Assignment receipt

The student acknowledges that the bachelor's thesis is an individual work. The student must produce his thesis without the assistance of others, with the exception of provided consultations. Within the bachelor's thesis, the author must state the names of consultants and include a list of references.

.	
Date of assignment receipt	Student's signature

Acknowledgements

I would like to thank my supervisor Ing. Denis Efremov for his valuable advice, guidance, and support during the creation of this thesis.

Great thanks also belong to the team of developers of the simulator "Live For Speed" which made it possible to implement this work.

I also thank Bc. Tomáš Twardzik and Bc. Adam Konopiský for the excellent help with the simulator for experimental tests and Bc.Bogdan Kashel for the exciting hours we spent testing the simulator.

Mainly I would like to thankmy parents and friends for their support and patience, without which this work would not be completed.

Abstrakt:

Cílem této bakalářské práce je definovat a zavést možné hierarchické řízení jízdní obálky. Jednostopý model s Pacejka Magic Formulou slouží jako konstrukční model vozidla a model pneumatik. Práce popisuje přizpůsobení konstrukčního modelu pro kontrolní účely a ukazuje výsledky pokusů na simulátoru dynamiky vozidla "Live For Speed". Na konci této práce bylo vytvořeno řízení boční obálky, které bylo otestováno na syntetických testech stejně jako na simulátoru s reálným řidičem.

Klíčová slova: Dynamika vozidla, Pacejka Magic Formula, Ochrana Jízdní Obálky, Steer-by-Wire, Stabilita Vozidla, Jednostopý Model, Řízení Uhlu Příčného Skluzu, Řízení Prokluz, Simulátor LFS.

Abstract:

This bachelor thesis aims to define and introduce possible hierarchical driving envelope protection control. The Single-Track model with Pacejka Magic formula serves as design vehicle and tire models. The work describes the design model's adaptation for the control purposes and shows experimental results provided on the vehicle dynamics simulator "Live for Speed." At the end of this work, control for lateral envelope was implemented and tested on synthetic and real driver ride tests.

Keywords: Vehicle Dynamics, Pacejka Magic Formula, Driving Envelope Protection, Steer-by-Wire, Vehicle Stability, Singel-Track Model, Side-Slip Angle Control, Slip Ratio Control, LFS Simulator.

Contents

1 Introduction **2**
1.1 Outline . . . 2

2 Objectives **3**

3 Used Vehicle Model **4**
3.1 Introduction . . . 4
3.2 Nonlinear Single-Track Model . . . 4
3.2.1 Modeling Assumptions . . . 4
3.2.2 Steering Angle Projection and Vehicle Dynamics . . . 4
3.3 Tire Modeling . . . 6
3.3.1 Simplified Pacejka Magic formula . . . 7
3.3.2 Side-Slip Angles . . . 7
3.3.3 Slip Ratios . . . 8

4 Driving Envelope Definition **9**
4.0.1 Lateral Envelope . . . 9
4.0.2 Longitudinal Envelope . . . 10
4.0.3 Combined Slip Envelope . . . 10

5 Single-Track Model Adaptation **11**
5.1 Introduction . . . 11
5.2 Identifying Pacejka Shaping Coefficients . . . 12
5.3 Longitudinal Dynamics Adaptation . . . 16
5.4 Lateral Dynamics Linearization . . . 17
5.5 Longitudinal Dynamics Linearization . . . 20
5.5.1 Throttle Input . . . 20
5.5.2 Brake Input . . . 23

6 Hierarchical Driving Envelope Protection **25**
6.1 Lateral Envelope . . . 25

7 Synthetic Ride Tests **27**
7.1 Slalom . . . 27
7.2 Aggressive Turn . . . 28

8 Real Driver Ride Tests **30**

9 Results **32**

10 Conclusion **33**

Bibliography **34**

List of Figures **35**

List of Tables **36**

1. Introduction

Nowadays, more and more smart advanced driver assistance systems are being created for the modern car, which provides safety and driving pleasure. One of the most advanced areas is the drive-by-wire car system. Thanks to this technology, we can help the driver to control the car in severe conditions or maneuvers while leaving him with a sense of complete control over the situation.

Since the drive-by-wire system was borrowed from the flight-control industry (fly-by-wire), along with it came its primary task: full-time-full-authority control, which aims to keep the vehicle within the driving envelope (envelope protection).

This thesis's primary goal is to develop a hierarchical control of the driving envelope using the vehicle from a simulator and make it possible to use not only in synthetic ride tests but also with the participation of a real driver in the simulator.

1.1 Outline

This work consists of ten main parts:

- Chapters [**Introduction**] and [**Objectives**] describe the work and its goals.
- Chapter [**Used Vehicle Model**] introduces used Single-Track and tire models.
- In part [**Driving Envelope Definition**] the Driving Envelope is defined from physical point of view.
- Part [**Single-Track Model Adaptation**] describes modifications made to the model for design purposes.
- Chapter [**Hierarchical Driving Envelope Protection**] introduces possible hierarchical lateral envelope protection.
- Part [**Synthetic Ride Tests**] describes implemented synthetic ride tests and checks the proposed control architecture.
- The final test of the implemented control is a comparison of a series of races in chapter [**Real Driver Ride Tests**] with the participation of a real driver.

2. Objectives

The main objectives of this thesis are:

- Define single-track and tire models and adapt them for design purposes.
- Study driving envelope definition and interpret it from physical point of view.
- Suggest suitable hierarchical control approach(-es) to protect boundaries defined by the driving envelope.
- Provide validation and verification ride test using racing simulator “Life for Speed”.
- Provide comparison of the controlled vehicle (with envelope protection algorithm) and driven vehicle by human.

3. Used Vehicle Model

3.1 Introduction

3.2 Nonlinear Single-Track Model

There are many ways to describe the vehicle dynamics, such as single-track, twin-track models, and others. For this thesis purposes, the single-track model is used due to fewer number of the states inside than the twin-track model and simpler implementation and validation processes.

3.2.1 Modeling Assumptions

The single-track model is a representation of planar or flat motion only. Therefore, some assumptions were made for this model:

- The mass of the car is assumed to be concentrated in one particular point, named center of gravity (CG).
- The mass distributed between the centers of the front and rear axles is assumed to be constant.
- All lifting, rolling, and pitching moments are considered negligible.
- The front and rear axles are represented as a single front and rear tire of the vehicle, respectively.
- All points of contact of the tire with the surface lie along the center of the axis
- Steering is only possible on the front axle
- The vehicle is driven with the front axle only
- Brakes are applied on both axles

3.2.2 Steering Angle Projection and Vehicle Dynamics

The coordinate system used to describe the position of the rigid body is shown in Figure 3.1. It represents the conventional right-hand Cartesian coordinate system. Looking at the Fig. 3.2 three degrees of freedom can be seen:

1. Lateral motion,
2. Longitudinal motion,
3. Yaw motion.

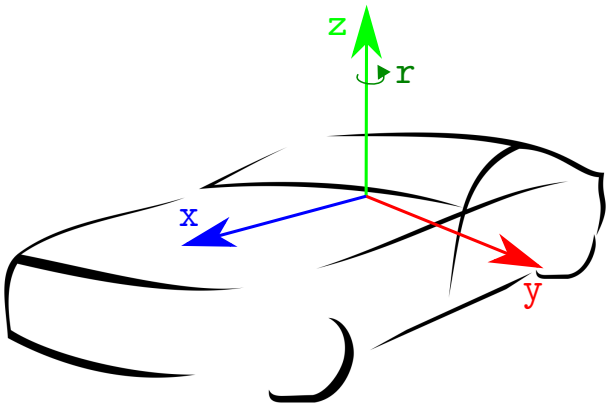

Figure 3.1: The vehicle coordinate system [2]

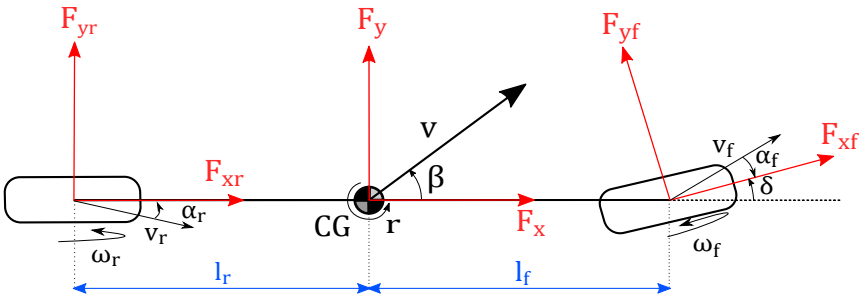

Figure 3.2: The single-track model in the selected coordinate system [8]

Now, the task is to obtain formulas that will describe the motions mentioned above. Velocity of the rigid body is characterized by the following system of equations:

$$\begin{aligned} v^2 &= v_{\mathrm{x}}^2 + v_{\mathrm{y}}^2, \\ v_{\mathrm{x}} &= v\cos(\beta), \\ v_{\mathrm{y}} &= v\sin(\beta), \end{aligned} \tag{3.1}$$

where v is a velocity of the body, v_{x} and v_{y} are velocities in the direction of the given axes, β is a side slip angle. Applying equation from [3]:

$$\begin{aligned} F_{\mathrm{x}} &= m(a_{\mathrm{x}} - rv_{\mathrm{y}}), \\ F_{\mathrm{y}} &= m(a_{\mathrm{y}} + rv_{\mathrm{x}}), \end{aligned} \tag{3.2}$$

where m is a mass of the vehicle, $a_{\mathrm{x}} = \dot{v}_{\mathrm{x}}$ and $a_{\mathrm{y}} = \dot{v}_{\mathrm{y}}$ are longitudinal and lateral accelerations, respectively, F_{x} and F_{y} are forces in given axes and r is a yaw rate. Eq 3.1 transforms into a system of equations that determine longitudinal and lateral motions of the single-track model, respectively:

$$\begin{aligned} F_{\mathrm{x}} &= -mv(\dot{\beta} + r)\sin\beta + m\dot{v}\cos\beta, \\ F_{\mathrm{y}} &= -mv(\dot{\beta} + r)\cos\beta + m\dot{v}\sin\beta. \end{aligned} \tag{3.3}$$

Yaw motion is characterized by the following equation:

$$M_z = I_z \dot{r}, \tag{3.4}$$

where M_z is a moment acting around the z axis, I_z is a moment of inertia of the vehicle around the z axis. From the equations 3.3 - 3.4 the following matrix equation can be written down:

$$\begin{pmatrix} \dot{\beta} \\ \dot{v} \\ \dot{r} \end{pmatrix} = \begin{pmatrix} \frac{1}{mv} & 0 & 0 \\ 0 & \frac{1}{m} & 0 \\ 0 & 0 & \frac{1}{I_z} \end{pmatrix} \begin{pmatrix} -\sin\beta & \cos\beta & 0 \\ \cos\beta & \sin\beta & 0 \\ 0 & 0 & 1 \end{pmatrix} \begin{pmatrix} F_{\mathrm{x}} \\ F_{\mathrm{y}} \\ M_z \end{pmatrix} - \begin{pmatrix} r \\ 0 \\ 0 \end{pmatrix}. \tag{3.5}$$

The forces F_{x} and F_{y} and the moment M_z can be also described by the following steering angle projection [2]

$$\begin{pmatrix} F_{\mathrm{x}} \\ F_{\mathrm{y}} \\ M_z \end{pmatrix} = \begin{pmatrix} \cos\delta & -\sin\delta & 1 & 0 \\ \sin\delta & \cos\delta & 0 & 1 \\ l_{\mathrm{f}}\sin\delta & l_{\mathrm{f}}\cos\delta & 0 & -l_{\mathrm{r}} \end{pmatrix} \begin{pmatrix} F_{\mathrm{xf}} \\ F_{\mathrm{yf}} \\ F_{\mathrm{xr}} \\ F_{\mathrm{yr}} \end{pmatrix}, \tag{3.6}$$

where δ is the steering angle, l_{f} is the distance from the vehicle's center of gravity to the front axle (the front wheel), and l_{r} is the distance from the vehicle's center of gravity to the rear axle (the rear wheel). Forces $F_{\mathrm{xf}}, F_{\mathrm{yf}}, F_{\mathrm{xr}}, F_{\mathrm{yr}}$ are defined in [**Tire Modelling**] section.

Eq 3.5 - 3.6 can be written as a matrix differential equation describing the steering angle projection and the vehicle dynamics:

$$\begin{aligned} \begin{pmatrix} f_1 \\ f_2 \\ f_3 \end{pmatrix} : \begin{pmatrix} \dot{\beta} \\ \dot{v} \\ \dot{r} \end{pmatrix} = & \begin{pmatrix} \frac{1}{mv} & 0 & 0 \\ 0 & \frac{1}{m} & 0 \\ 0 & 0 & \frac{1}{I_z} \end{pmatrix} \begin{pmatrix} -\sin\beta & \cos\beta & 0 \\ \cos\beta & \sin\beta & 0 \\ 0 & 0 & 1 \end{pmatrix} \\ & \begin{pmatrix} \cos\delta & -\sin\delta & 1 & 0 \\ \sin\delta & \cos\delta & 0 & 1 \\ l_{\mathrm{f}}\sin\delta & l_{\mathrm{f}}\cos\delta & 0 & -l_{\mathrm{r}} \end{pmatrix} \begin{pmatrix} F_{\mathrm{xf}} \\ F_{\mathrm{yf}} \\ F_{\mathrm{xr}} \\ F_{\mathrm{yr}} \end{pmatrix} - \begin{pmatrix} r \\ 0 \\ 0 \end{pmatrix}. \end{aligned} \tag{3.7}$$

3.3 Tire Modeling

One of the most important characteristics in vehicle dynamics simulation is a tire model. Therefore, there are many methods that differ in accuracy and the number of required parameters, the most famous of which, proposed by Hans Bastian Pacejka, has 20 different coefficients [10]. The Simplified Pacejka Magic formula [10] is used as it has smaller number of coefficients, simpler calculation, and the same formula is used to estimate the lateral and longitudinal forces applied on a tire.

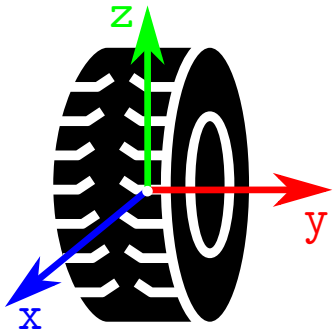

Figure 3.3: The tire coordinate system.

3.3.1 Simplified Pacejka Magic formula

General view of the Simplified Pacejka Magic formula is:

$$F_{\mathrm{yf}}(s) = c_{\mathrm{D,y}} F_{\mathrm{zf}} \sin(c_{\mathrm{C,y}} \arctan(c_{\mathrm{B,y}}\alpha_{\mathrm{f}} - c_{\mathrm{E,y}}(c_{\mathrm{B,y}}\alpha_{\mathrm{f}} - \arctan(c_{\mathrm{B,y}}\alpha_f)))), \tag{3.8}$$

where F_{yf} is a lateral force on the front tire, α_f is a side-slip angle of the front tire (see [**Side-slip angles**]), F_{zf} is a vertical load of the tire in the front, coefficients of Pacejka formula are responsible for the following settings:

- $c_{\mathrm{D,y}}$ peak value of the curve,
- $c_{\mathrm{C,y}}$ shape around the peak value,
- $c_{\mathrm{B,y}}$ stiffness factor,
- $c_{\mathrm{E,y}}$ curvature factor.

The same formula (with different Pacejka coefficients) can be used for calculation of $F_{\mathrm{yr}}, F_{\mathrm{xf}}, F_{\mathrm{xr}}$ tire forces if the α_f is replaced with the $\alpha_{\mathrm{r}}, \lambda_{\mathrm{f}}, \lambda_{\mathrm{r}}$ (see [**Slip ratios**]), respectively.

3.3.2 Side-Slip Angles

Applying equations from [3]:

$$\alpha_{\mathrm{f}} = -\arctan\left(\frac{v_{\mathrm{yf}}}{|v_{\mathrm{xf}}|}\right), \tag{3.9}$$

$$\begin{pmatrix} v_{\mathrm{xf}} \\ v_{\mathrm{yf}} \end{pmatrix} = \begin{pmatrix} \cos\delta & \sin\delta \\ -\sin\delta & \cos\delta \end{pmatrix} \begin{pmatrix} v_x \\ v_y + l_{\mathrm{f}} r \end{pmatrix} = \begin{pmatrix} \cos\delta & \sin\delta \\ -\sin\delta & \cos\delta \end{pmatrix} \begin{pmatrix} v\cos\beta \\ v\sin\beta + l_{\mathrm{f}} r \end{pmatrix}, \tag{3.10}$$

where $v_{\mathrm{xf}}, v_{\mathrm{yf}}$ are components of velocity v_f sharing same direction as $F_{\mathrm{xf}}, F_{\mathrm{yf}}$, respectively (Fig. 3.3), the tire side-slip angle α_f is defined as:

$$\begin{aligned} \alpha_{\mathrm{f}} &= -\arctan\frac{(v\sin\beta + l_{\mathrm{f}} r)\cos\delta_f - v\cos\beta\sin\delta_f}{|(v\sin\beta + l_{\mathrm{f}} r)\sin\delta_f + v\cos\beta\cos\delta_f|} = \\ &= -\arctan\frac{(v_{\mathrm{y}} + l_{\mathrm{f}} r)\cos\delta_f - v_{\mathrm{x}}\sin\delta_f}{|(v_{\mathrm{y}} + l_{\mathrm{f}} r)\sin\delta_f + v_{\mathrm{x}}\cos\delta_f|} \end{aligned} \tag{3.11}$$

For rear tires, using the assumptions given earlier, the equation takes the following form:

$$\begin{aligned} \alpha_{\mathrm{r}} &= -\arctan\left(\frac{v_{\mathrm{yr}}}{|v_{\mathrm{xr}}|}\right), \\ \begin{pmatrix} v_{\mathrm{xr}} \\ v_{\mathrm{yr}} \end{pmatrix} &= \begin{pmatrix} 1 & 0 \\ 0 & 1 \end{pmatrix} \begin{pmatrix} v_{\mathrm{x}} \\ v_{\mathrm{y}} - l_{\mathrm{r}} r \end{pmatrix} = \begin{pmatrix} 1 & 0 \\ 0 & 1 \end{pmatrix} \begin{pmatrix} v\cos\beta \\ v\sin\beta - l_{\mathrm{r}} r \end{pmatrix}, \end{aligned} \tag{3.12}$$

where $v_{\mathrm{xr}}, v_{\mathrm{yr}}$ are components of velocity v_r sharing same direction as $F_{\mathrm{xr}}, F_{\mathrm{yr}}$, respectively (Fig. 3.3), the tire side-slip angle α_{r} is defined as:

$$\alpha_{\mathrm{r}} = -\arctan\left(\frac{v_{\mathrm{y}} - l_{\mathrm{r}} r}{|v_{\mathrm{x}}|}\right) = -\arctan\left(\frac{v\sin\beta - l_{\mathrm{r}} r}{|v\cos\beta|}\right). \tag{3.13}$$

3.3.3 Slip Ratios

Slip ratios are characterized by following equations [3]:

$$\lambda_{\mathrm{f}} = \frac{\omega_{\mathrm{f}} p - v_{\mathrm{xf}}}{\max(|\omega_{\mathrm{f}} p|, |v_{\mathrm{xf}}|)}, \tag{3.14}$$

$$\lambda_{\mathrm{r}} = \frac{\omega_{\mathrm{r}} p - v_{\mathrm{xr}}}{\max(|\omega_{\mathrm{r}} p|, |v_{\mathrm{xr}}|)}, \tag{3.15}$$

where $\lambda_{\mathrm{f}}, \lambda_{\mathrm{r}}$ are a slip ratios on the front and rear tire respectively, ω_{f} is a tire angular velocity and p is a radius of a tire. Notice that according to the definition, slip ratios are bounded on the interval $[-1, 1]$.

4. Driving Envelope Definition

The Driving Envelope (DE) [4] is defined as a combination of capacity boundaries for each wheel (front and rear for single-track model) and there are three conditions, which are considered:

- Lateral envelope - boundaries for the side-slip angles $\alpha_{f/r}$,
- Longitudinal envelope - boundaries for the slip ratios $\lambda_{f/r}$,
- Combined slip envelope - boundary for the combined slip defined with the traction ellipse.

4.0.1 Lateral Envelope

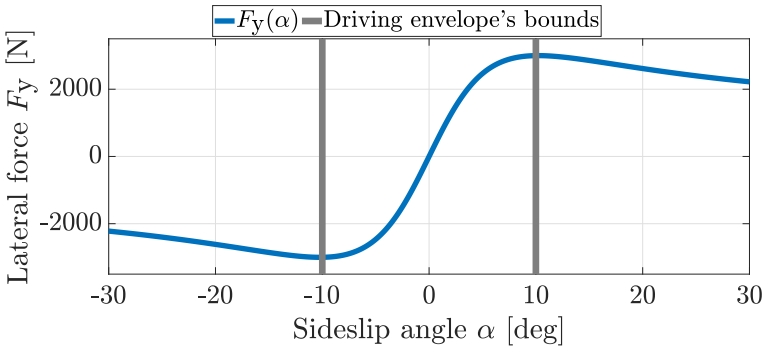

Figure 4.1: DE definition for longitudinal dynamic [4].

In the relation graph (Fig. 4.1) between the side-slip angle α and the produced lateral force F_y there are three states to the mansion:

1. The first state concerns the plot area, where the side-slip angle value is located between the selected peaks of maximum and minimum lateral force values. In this part, the relation of the variables is near-to-linear.
2. When the produced lateral force decreases after its maximum peak and then saturates, the side-slip angle continues to increase and the tyre loses its grip on the surface, resulting to uncontrolled rotation or sliding.
3. The third condition is symmetrical to the second but applies to negative values of the lateral force and side-slip angles.

To sum up, the most effective and controllable state can be described by the following expression:

$$\begin{aligned} \alpha_{\mathrm{f,min}} \leq \alpha_{\mathrm{f}} \leq \alpha_{\mathrm{f,max}}, \\ \alpha_{\mathrm{r,min}} \leq \alpha_{\mathrm{r}} \leq \alpha_{\mathrm{r,max}}. \end{aligned} \tag{4.1}$$

4.0.2 Longitudinal Envelope

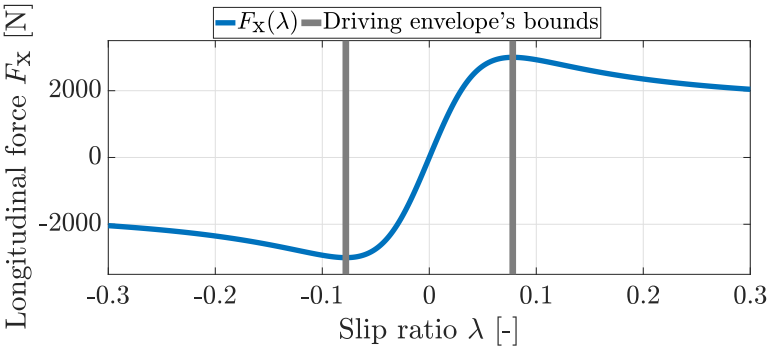

Figure 4.2: DE definition for longitudinal dynamic [4]

.

A similar situation shown in Fig. 4.1 is observed in the graph of the longitudinal force F_x and the slip ratio λ relation (Fig. 4.2). Boundaries for the longitudinal envelope are:

$$\begin{aligned} \lambda_{\mathrm{f,min}} \leq \lambda_{\mathrm{f}} \leq \lambda_{\mathrm{f,max}}, \\ \lambda_{\mathrm{r,min}} \leq \lambda_{\mathrm{r}} \leq \lambda_{\mathrm{r,max}}. \end{aligned} \tag{4.2}$$

4.0.3 Combined Slip Envelope

The lateral and longitudinal envelopes are defined separately from each other, without taking into account the fact that a total force generated on the tire can not be higher than the μF_z, where μ is a friction coefficient of a road surface [5].

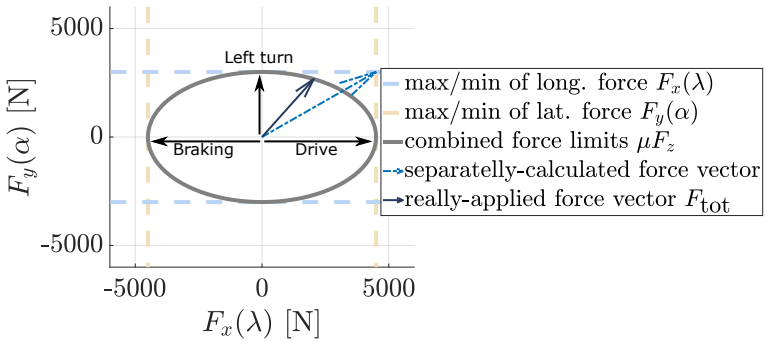

Figure 4.3: Combined tire force limits [4]

.

A combined slip occurs when the vehicle accelerates or brakes in a turning maneuver. The total force is shown in Fig. 4.3 and defined as [4]:

$$F_{\mathrm{tot}} = \sqrt{\frac{F_{\mathrm{x}}^2}{c_{\mathrm{D,x}}^2} + \frac{F_{\mathrm{y}}^2}{c_{\mathrm{D,y}}^2}} \leq \mu F_{\mathrm{z}}. \tag{4.3}$$

5. Single-Track Model Adaptation

5.1 Introduction

The "Live for Speed" racing simulator [7] is used to test out simulation experiments, hierarchical control, and provide synthetic and real driver ride tests. Available input and output signals are listed in Tables 5.1 and 5.2. For the above purposes, a specific car named XF GTR was selected in the simulator, which has constant parameters shown in Table 5.3. The simulator has input signals different from the inputs of the single-track model [**Used Vehicle Model**] and does not provide any information about Pacejka coefficients. Therefore, this chapter focuses on offering adopting functions between the model and simulator and the identification of unknown parameters.

Table 5.1: Inputs of the simulator

Input	Symbol	Range of values
Steering wheel	θ	$[-1, 1]$
Throttle pedal	p_{t}	$[0, 1]$
Brake pedal	p_{b}	$[0, 1]$

Table 5.2: Used outputs of the simulator

Output	Symbol	Units
Number of the gear that is currently engaged	g_{n}	$-$
Yaw rate	r	$\mathrm{rad\,s^{-1}}$
Longitudinal velocity of the CG point	v_{x}	$\mathrm{m\,s^{-1}}$
Lateral velocity of the CG point	v_{y}	$\mathrm{m\,s^{-1}}$
Longitudinal force of the left front wheel	F_{xlf}	N
Lateral force of the left front wheel	F_{ylf}	N
Vertical Load of the left front wheel	F_{zlf}	N
Slip ratio of the left front wheel	λ_{lf}	$-$
Side-slip angle of the left front wheel	α_{lf}	rad
Angular velocity of the left front wheel	ω_{lf}	$\mathrm{rad\,s^{-1}}$
Longitudinal force of the right front wheel	F_{xrf}	N
Lateral force of the right front wheel	F_{yrf}	N
Vertical Load of the right front wheel	F_{zrf}	N
Slip ratio of the right front wheel	λ_{rf}	rad
Side-slip angle of the right front wheel	α_{rf}	rad
Angular velocity of the right front wheel	ω_{rf}	$\mathrm{rad\,s^{-1}}$
Angular velocity of the engine	ω_{e}	$\mathrm{rad\,s^{-1}}$

Table 5.3: Available constant parameters of the vehicle

Parameter	Symbol	Value	Units
Vehicle mass	m	840	kg
Yaw moment of inertia	I_z	2600	$\mathrm{kg\,m^{-2}}$
Moment of inertia of wheels	I_w	0.5	$\mathrm{kg\,m^2}$
Maximum steering wheel lock	δ_max	0.42	rad
Front axle-CG distance	l_f	0.93	m
Rear axle-CG distance	l_r	1.35	m
Radius of wheels	p	0.2765	m
Brake balance	b_b	0.85	-
Brake strength	b_s	780	-
First gear ratio	g_1	3.3	-
Second gear ratio	g_2	2.4	-
Third gear ratio	g_3	1.9	-
Fourth gear ratio	g_4	1.5	-
Fifth gear ratio	g_5	1.22	-
Sixth gear ratio	g_6	1	-
Final drive ratio	g_final	3.2	-
Transmission efficiency	η	0.85	-
Rolling resistance coefficient	k	0.015	$\mathrm{rad\,kg^{-1}\,m^{-1}}$
Maximum engine torque	τ_max	307.040	N m
Torque spread half	τ_sh	717.568	N m
Engine angular velocity at maximum engine torque	$\omega_{\tau_\mathrm{max}}$	652.335	$\mathrm{rad\,s^{-1}}$

5.2 Identifying Pacejka Shaping Coefficients

All experiments in this subsection consider the forces on the rear wheels of the vehicle as negligible. Measuring the F_ylf, F_yrf, α_lf, and α_rf, it is possible to identify Pacejka coefficients for lateral dynamics. Input parameters of the simulator for the identification are shown in Fig 5.1. For the convenience of calculation, output signals of the simulator are modified using a system of equations 5.1 in this experiment since the applied single-track model does not distinguish between the right and left wheels.

$$\begin{aligned} \alpha_\mathrm{f} &= \frac{\alpha_\mathrm{lf} + \alpha_\mathrm{rf}}{2}, \\ F_\mathrm{yf} &= F_\mathrm{ylf} + F_\mathrm{yrf}, \\ F_\mathrm{zf} &= F_\mathrm{zlf} + F_\mathrm{zrf}. \end{aligned} \tag{5.1}$$

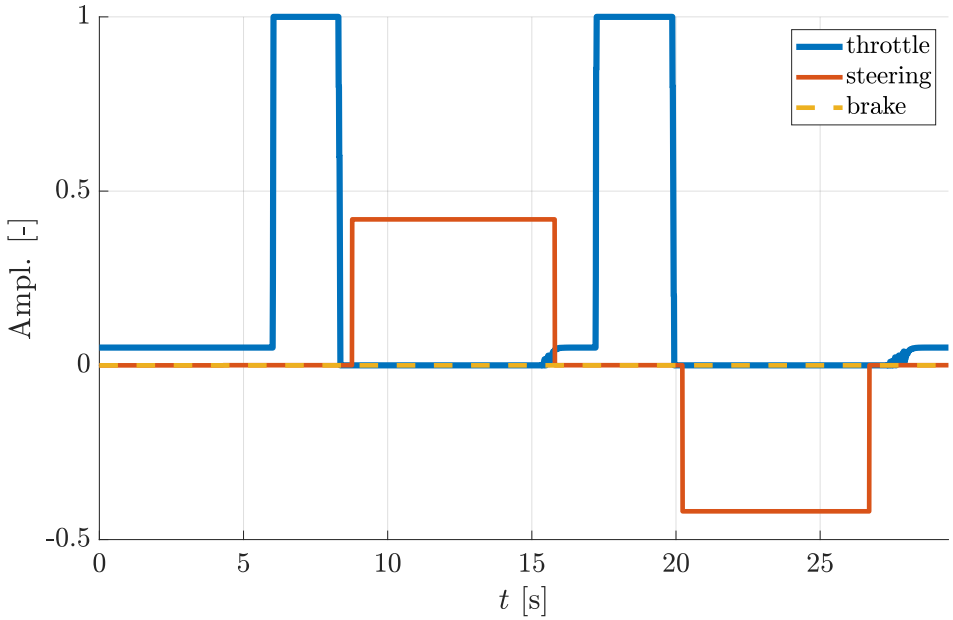

Figure 5.1: Input signals for the Pacejka coefficients for lateral dynamics identification.

Only data from the green area (Fig. 5.2) are used for further calculations to reduce the amount of repetitive data and the impact of noise.

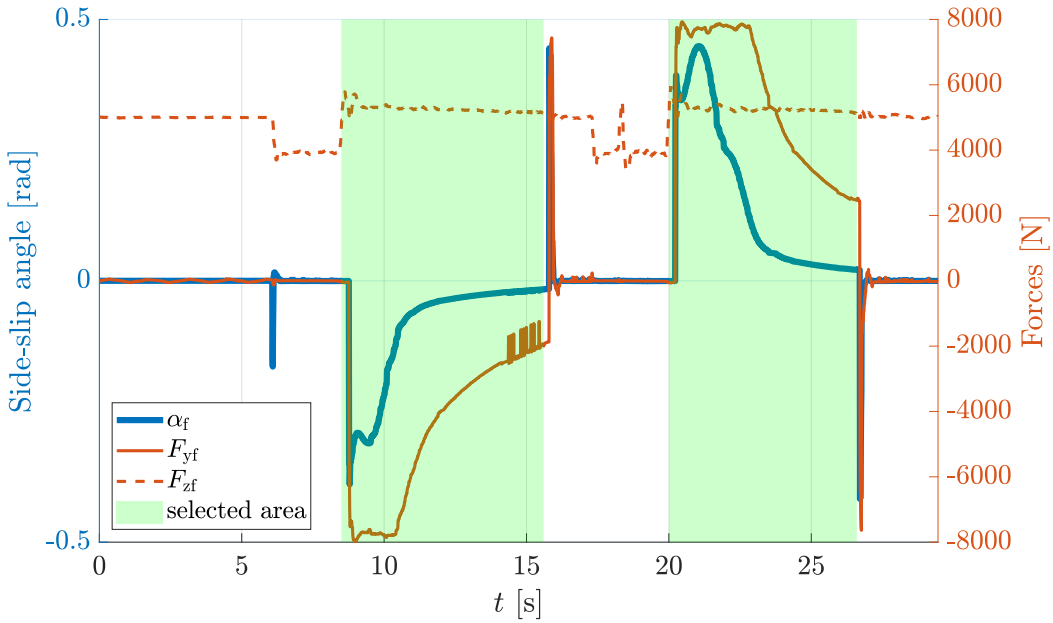

Figure 5.2: Selected signals for the Pacejka coefficients for lateral dynamics identification.

Using robust fitting algorithm [6], the fitted Pacejka formula (Eq. 3.8) for lateral dynamics takes the form shown in Fig. 5.3.

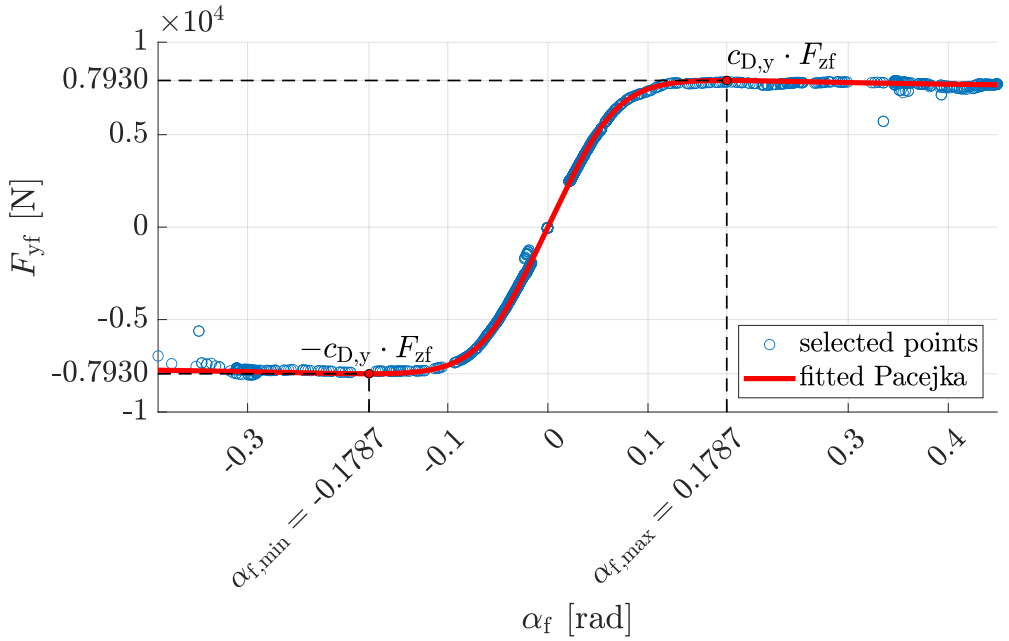

Figure 5.3: Identified Pacejka formula for lateral dynamics.

During experiments on the Pacejka formula for longitudinal dynamics, it became clear that the physics of braking in the simulator works differently than on the single-track. It will be assumed that the curve for the longitudinal dynamic will be mirrored (Fig. 5.6) as in the case of lateral dynamics. Input signals for the identification of Pacejka coefficients for longitudinal dynamics are shown in Fig 5.1.

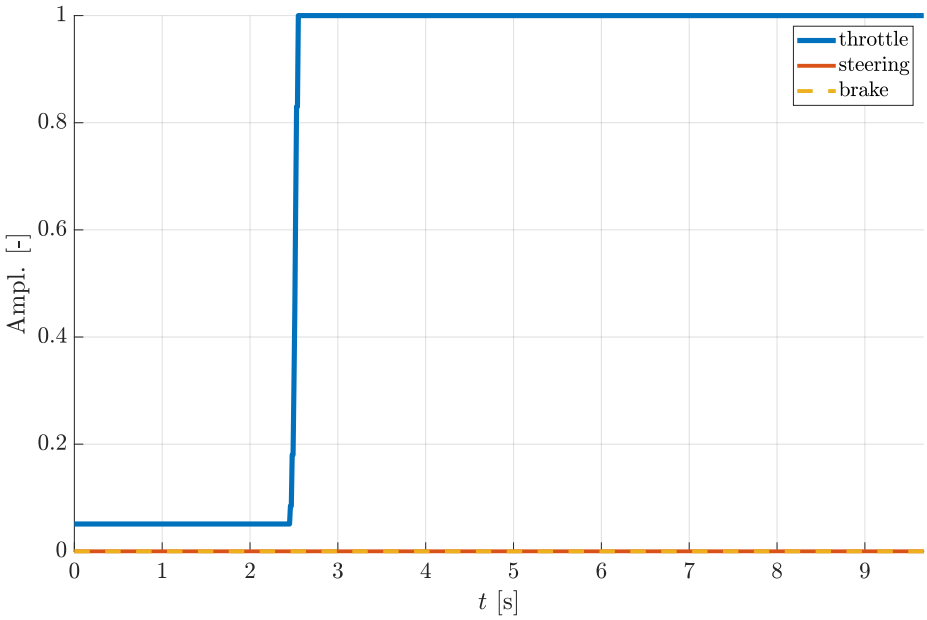

Figure 5.4: Input signals for the Pacejka coefficients for longitudinal dynamics identification.

For the same reason as in the previous experiment, only selected data are used for onward identification (Fig. 5.5). Output signals of the simulator are modified using a

system of equations 5.2 likewise in the previous experiment.

$$\begin{aligned} \lambda_{\mathrm{f}} &= \frac{\lambda_{\mathrm{lf}} + \lambda_{\mathrm{rf}}}{2}, \\ F_{\mathrm{xf}} &= F_{\mathrm{xlf}} + F_{\mathrm{xrf}}, \\ F_{\mathrm{zf}} &= F_{\mathrm{zlf}} + F_{\mathrm{zrf}}. \end{aligned} \tag{5.2}$$

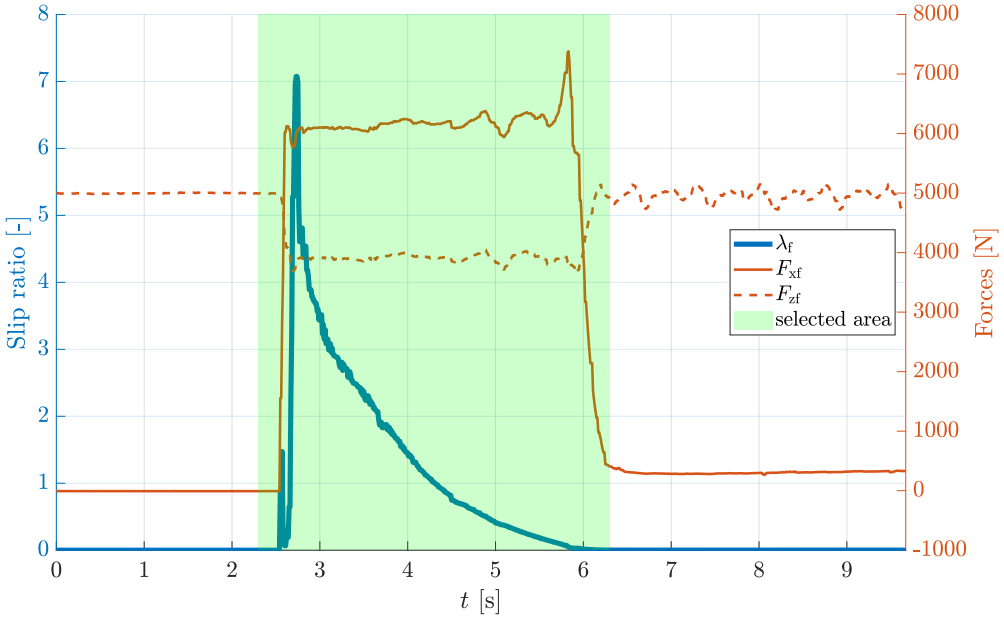

Figure 5.5: Selected output signals for the Pacejka coefficients for longitudinal dynamics identification.

Using the same method as in the earlier identification, the fitted Pacejka formula for longitudinal dynamics takes the form shown in Fig. 5.6.

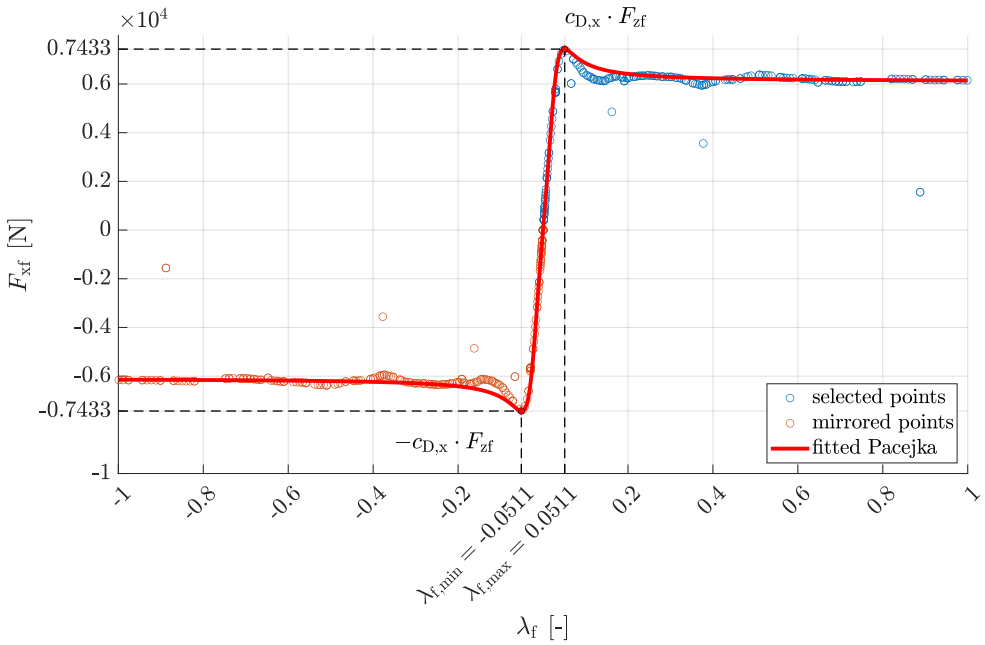

Figure 5.6: Identified Pacejka formula for longitudinal dynamics.

In conclusion, identified coefficients for lateral and longitudinal dynamics are presented in Table 5.4.

Table 5.4: Identified Pacejka coefficients for lateral dynamics.

Coefficient	Value
$c_{\mathrm{D,y}}$	1.5069
$c_{\mathrm{C,y}}$	1.2302
$c_{\mathrm{B,y}}$	11.5594
$c_{\mathrm{E,y}}$	-1.3182
$c_{\mathrm{D,x}}$	1.8333
$c_{\mathrm{C,x}}$	1.3885
$c_{\mathrm{B,x}}$	20.4812
$c_{\mathrm{E,x}}$	-4.7089

5.3 Longitudinal Dynamics Adaptation

To control the longitudinal dynamics of the car, it is necessary to expand the previously given system with another state. The control will be performed using the throttle and brake pedals, which is not available in the standard single-track model. A front wheel (both left and right) has an internal state that describes its rotation acceleration and is defined by the differential equation 5.3 [3].

$$\dot{\omega}_{\mathrm{f}} = \frac{1}{I_{\mathrm{w}}}(\tau_{\mathrm{df}} - pF_{\mathrm{xf}} - \mathrm{sign}(\omega_{\mathrm{f}})\tau_{\mathrm{bf}}) - kF_{\mathrm{zf}}, \tag{5.3}$$

where τ_{df} is a drive torque of the front tire, τ_{bf} is a brake torque of the front tire. The system of equations below is a bell-shaped function (Fig. 5.7) of the dependence of engine torque on engine angular velocity. The Eq. 5.4 was provided by the developers of the simulator [7], as the engine's implementation significantly changes the approach to linearization and control of all longitudinal dynamics.

$$\begin{aligned} \tau_{\mathrm{df}} &= g_{\mathrm{g_n}} g_{\mathrm{final}} \eta \tau_{\mathrm{e}}, \\ \tau_{\mathrm{e}} &= \frac{\tau_{\max}}{1 + \left(\frac{\omega_{\mathrm{e}} - \omega_{\tau_{\max}}}{\tau_{\mathrm{sh}}}\right)^2} p_{\mathrm{t}}, \\ \omega_{\mathrm{e}} &= g_{\mathrm{g_n}} g_{\mathrm{final}} \omega_{\mathrm{f}}, \\ \tau_{\mathrm{bf}} &= 2 b_{\mathrm{b}} b_{\mathrm{s}} p_{\mathrm{b}}. \end{aligned} \tag{5.4}$$

where τ_{e} is an engine torque.

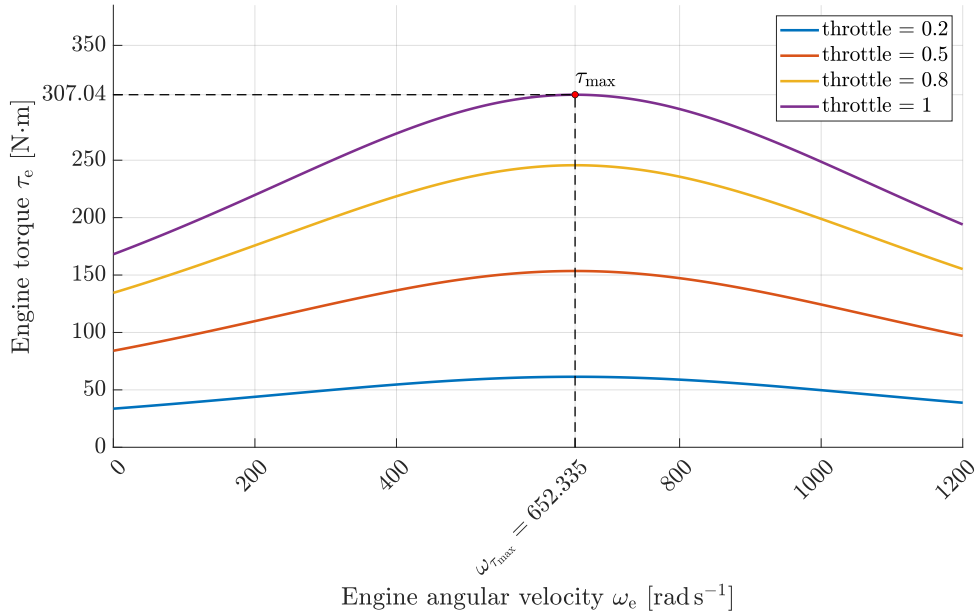

Figure 5.7: Bell-shaped dependency between engine torque and engine angular velocity.

5.4 Lateral Dynamics Linearization

The Single-Track model (Eq. 3.7) is entirely suitable for further linearization and doesn't need to be adapted. The following assumptions are assumed:

- $v = v_{\mathrm{c}}$ is constant.
- ω_{f} is constant.
- $\dot{v} = 0$.
- $\sin x \approx x$.
- $\cos x \approx 1$.

- $\beta^2 \ll 1$.

Applying assumptions to the non-linear single-track model, a new system of equations was created:

$$\begin{aligned}
\dot{\beta} &= -\frac{1}{mv_\mathrm{c}}\beta F_\mathrm{x} + \frac{1}{mv_\mathrm{c}}F_\mathrm{y} - r, \\
\dot{r} &= \frac{1}{I_\mathrm{z}}M_\mathrm{z}, \\
F_\mathrm{x} &= -\beta F_\mathrm{y}, \\
F_\mathrm{y} &= F_\mathrm{xf}\delta + F_\mathrm{yf} + F_\mathrm{yr}, \\
M_\mathrm{z} &= F_\mathrm{xf}l_\mathrm{f}\delta + F_\mathrm{yf}l_\mathrm{f} - F_\mathrm{yr}l_\mathrm{r}.
\end{aligned} \tag{5.5}$$

The slip angles α_f, α_r and the slip ratio λ_f can also be linearized [5]:

$$\begin{aligned}
\alpha_\mathrm{f} &= \delta - \beta - \frac{l_\mathrm{f}r}{v_\mathrm{c}}, \\
\alpha_\mathrm{r} &= -\beta + \frac{l_\mathrm{r}r}{v_\mathrm{c}}, \\
\lambda_\mathrm{f} &= \frac{p\omega_\mathrm{f}}{v_\mathrm{c}} - 1.
\end{aligned} \tag{5.6}$$

The lateral forces F_yf, F_yr and longitudinal forces F_xf acting on each tire can be estimated (Fig. 5.8) by linear Two-Lines tire model [9] as:

$$\begin{aligned}
F_\mathrm{yf} &= c_\mathrm{yf}\alpha_\mathrm{f}, \\
F_\mathrm{yr} &= c_\mathrm{yr}\alpha_\mathrm{r}, \\
F_\mathrm{xf} &= c_\mathrm{xf}\lambda_\mathrm{f}, \\
F_\mathrm{xr} &= c_\mathrm{xr}\lambda_\mathrm{r},
\end{aligned} \tag{5.7}$$

where

$$\begin{aligned}
c_\mathrm{xf} &= c_\mathrm{D,x}c_\mathrm{B,x}c_\mathrm{C,x}F_\mathrm{zf}, \\
c_\mathrm{xr} &= c_\mathrm{D,x}c_\mathrm{B,x}c_\mathrm{C,x}F_\mathrm{zr}, \\
c_\mathrm{yf} &= c_\mathrm{D,y}c_\mathrm{B,y}c_\mathrm{C,y}F_\mathrm{zf}, \\
c_\mathrm{yr} &= c_\mathrm{D,y}c_\mathrm{B,y}c_\mathrm{C,y}F_\mathrm{zr}, \\
F_\mathrm{zf} &= gm\frac{l_\mathrm{r}}{l_\mathrm{r}+l_\mathrm{f}}, \\
F_\mathrm{zr} &= gm\frac{l_\mathrm{f}}{l_\mathrm{r}+l_\mathrm{f}},
\end{aligned} \tag{5.8}$$

where g is a gravitational constant.

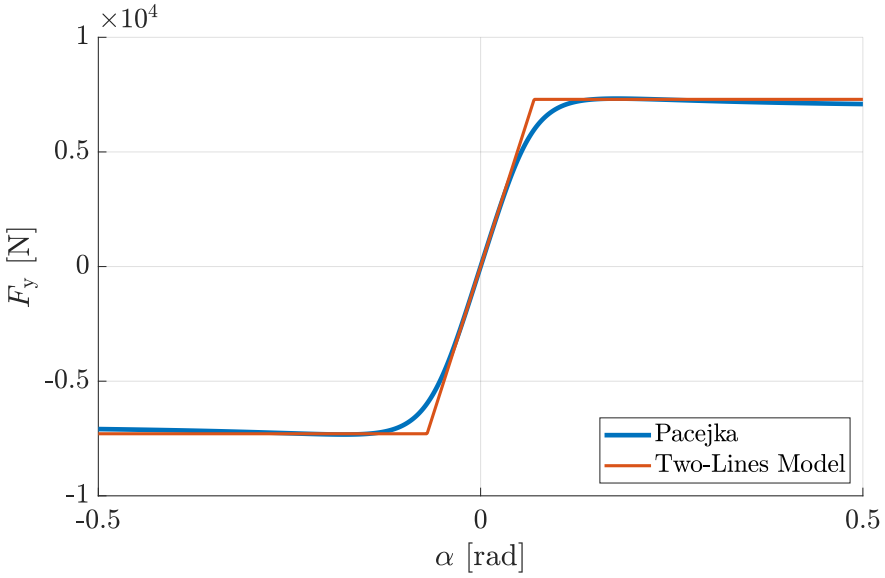

Figure 5.8: Compirison of Pacejka and Two-Lines tire models.

The state-space representation can be written in matrix form as:

$$\begin{pmatrix} \dot{\beta} \\ \dot{r} \end{pmatrix} = \begin{pmatrix} -\frac{c_{\mathrm{xf}}+c_{\mathrm{xr}}}{m v_{\mathrm{c}}} & \frac{l_{\mathrm{r}} c_{\mathrm{xr}} - l_{\mathrm{f}} c_{\mathrm{xf}}}{m v_{\mathrm{c}}^2} - 1 \\ \frac{l_{\mathrm{r}} c_{\mathrm{xr}} - l_{\mathrm{f}} c_{\mathrm{xf}}}{I_{\mathrm{z}}} & -\frac{l_{\mathrm{f}}^2 c_{\mathrm{xf}} + l_{\mathrm{r}}^2 c_{\mathrm{xr}}}{v_{\mathrm{c}} I_{\mathrm{z}}} \end{pmatrix} \begin{pmatrix} \beta \\ r \end{pmatrix} + \begin{pmatrix} \frac{c_{\mathrm{xf}}}{m v_{\mathrm{c}}} \\ \frac{l_{\mathrm{f}} c_{\mathrm{xf}}}{I_{\mathrm{z}}} \end{pmatrix} \delta. \tag{5.9}$$

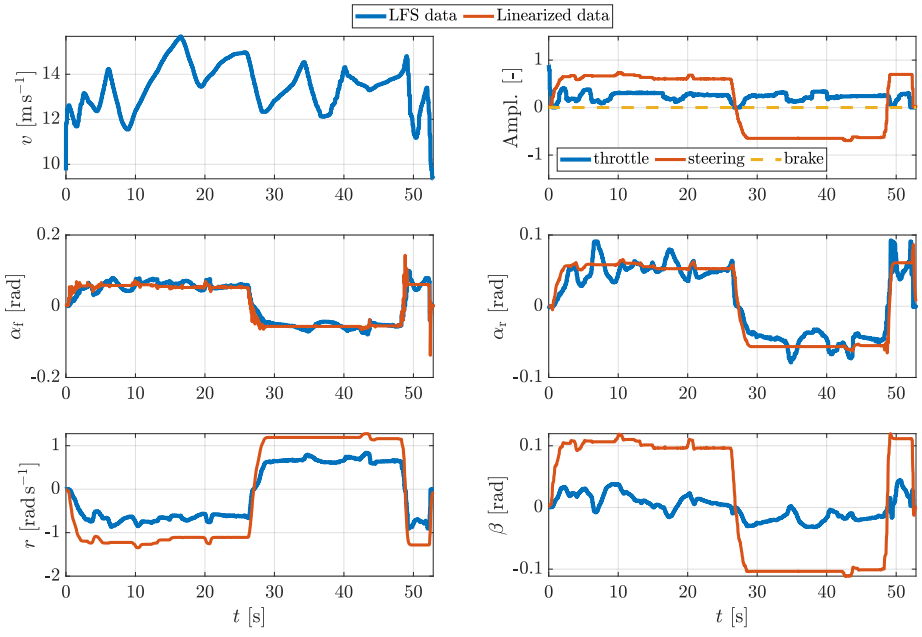

Figure 5.9: Comparison of a linearized system with the LFS simulator at constant velocity $v_{\mathrm{c}} = 10$ [m·s^{-1}]

A comparison of the linearized system (Fig. 5.9) shows that the approximated side-slip angle coincides with the simulated data with a deviation of about 5 [m·s^{-1}] from the operating point. Thus, the subsequent control should be performed for several linearized

systems, which will be calculated for working points in increments of 5 [m·s^{-1}].

5.5 Longitudinal Dynamics Linearization

The linearized longitudinal model will be divided into two parts separately for the throttle pedal and the brake pedal. Thus, it will be assumed that both of these pedals cannot be engaged simultaneously.

5.5.1 Throttle Input

Assuming the driving torque is engaged and the braking torque is zero, equation 5.3 transforms into a more straightforward equation 5.10.

$$\dot{\omega}_\mathrm{f} = \frac{1}{I_\mathrm{w}}(\tau_\mathrm{df} - pF_\mathrm{xf}) - kF_\mathrm{zf}. \tag{5.10}$$

For the drive torque τ_df, assume that the velocity of the vehicle $v = v_\mathrm{c}$ is constant. Therefore, the angular velocity of the engine and wheels is also constant and the following substitution

$$\omega_\mathrm{f} = \frac{v_\mathrm{c}}{p}, \tag{5.11}$$

along with the assumption changes equation 5.4 as follows:

$$\tau_\mathrm{df} = g_\mathrm{gn} g_\mathrm{final} \eta \frac{\tau_\mathrm{max}}{1 + \left(\frac{g_\mathrm{gn} g_\mathrm{final} \frac{v_\mathrm{c}}{p} - \omega_{\tau_\mathrm{max}}}{\tau_\mathrm{sh}} \right)^2} p_\mathrm{t}. \tag{5.12}$$

fig 4.10 check the y-axis and graph colors The longitudinal force F_xf and vertical load force F_zf are linearized in the same way as in equation 5.7. The result is a linear equation with an affine term:

$$\begin{aligned}
\dot{\omega}_\mathrm{f} &= A_\mathrm{t}\omega_\mathrm{f} + B_\mathrm{t}p_\mathrm{t} + d_\mathrm{t}, \\
B_\mathrm{t} &= \left(\frac{g_\mathrm{gn} g_\mathrm{final} \eta}{I_\mathrm{w}} \frac{\tau_\mathrm{max}}{1 + \left(\frac{g_\mathrm{gn} g_\mathrm{final} \frac{v_\mathrm{c}}{p} - \omega_{\tau_\mathrm{max}}}{\tau_\mathrm{sh}} \right)^2} \right), \\
A_\mathrm{t} &= \left(-\frac{p^2 c_\mathrm{xf}}{I_\mathrm{w} v_\mathrm{c}} \right), \\
d_\mathrm{t} &= \left(-\frac{p c_\mathrm{xf}}{I_\mathrm{w}} - kF_\mathrm{zf} \right).
\end{aligned} \tag{5.13}$$

The lookup table (5.5) was created based on a graph of speed and gear number measurements (5.10) to leave gear gain independent on time.

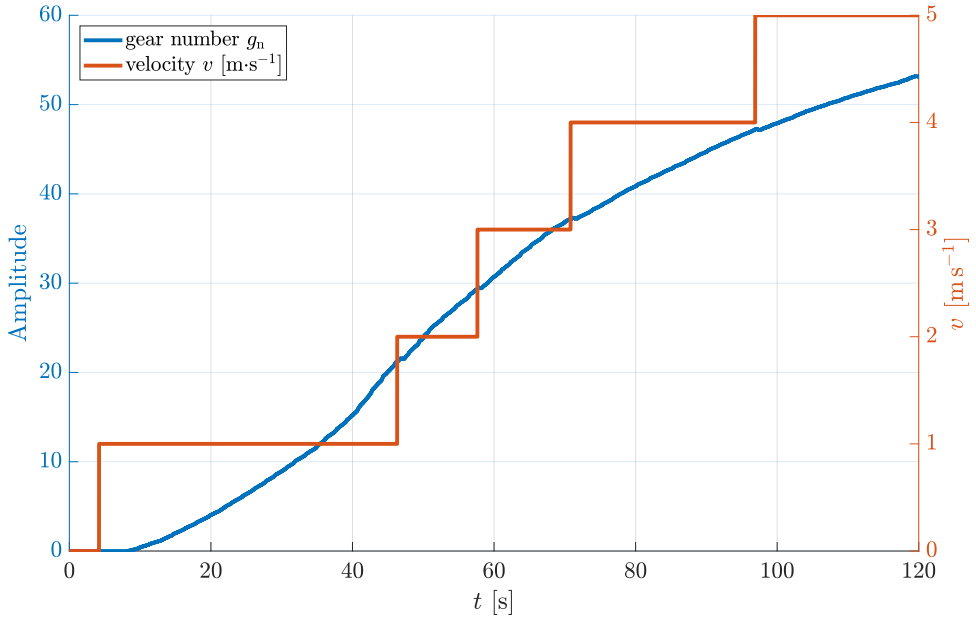

Figure 5.10: The dependency of the transmission number on the speed of the vehicle

Table 5.5: Lookup table for the gear gain of the linearized system.

Gear number g_n	Velocity interval of the vehicle v [m·s^{-1}]
1	0 - 21,5
2	21,5 - 30
3	30 - 37
4	37 - 47
5	47 - ∞

For further control of the system, it is necessary to get rid of the affine term. A substitution will be set up for this purpose:

$$\begin{aligned} \omega_{\mathrm{t,lin}} &= \omega_{\mathrm{f}} + \frac{d_{\mathrm{t}}}{A_{\mathrm{t}}}, \\ \dot{\omega}_{\mathrm{t,lin}} &= \dot{\omega}_{\mathrm{f}}. \end{aligned} \tag{5.14}$$

The desired system output, namely the slip ratio, is also changed to fit the substitution:

$$\begin{aligned} \lambda_{\mathrm{f}} &= \frac{p}{v_{\mathrm{c}}}\omega_{\mathrm{f}} - 1 = C_{\mathrm{t}}\omega_{\mathrm{t,lin}} + e_{\mathrm{t}}, \\ C_{\mathrm{t}} &= \frac{p}{v_{\mathrm{c}}}, \\ e_{\mathrm{t}} &= \left(-\frac{pd_{\mathrm{t}}}{Av_{\mathrm{c}}} - 1\right), \end{aligned} \tag{5.15}$$

The resulted state-space representation is:

$$\begin{aligned} \dot{\omega}_{\mathrm{t,lin}} &= A_{\mathrm{t}}\omega_{\mathrm{t,lin}} + B_{\mathrm{t}}p_{\mathrm{t}}, \\ \lambda_{\mathrm{t,lin}} &= C_{\mathrm{t}}\omega_{\mathrm{t,lin}} \end{aligned} \tag{5.16}$$

When comparing the modeled systems (Fig. 5.11), a problem was identified. The wheels' angular speeds coincide at the operating point, and the nonlinear model behaves identically to the LFS simulator. However, when calculating the slip ratio, it is clear that the linearized model has a significant difference compared to the simulator. The nonlinear model is noisy, but this problem is observed only at low speeds during acceleration.

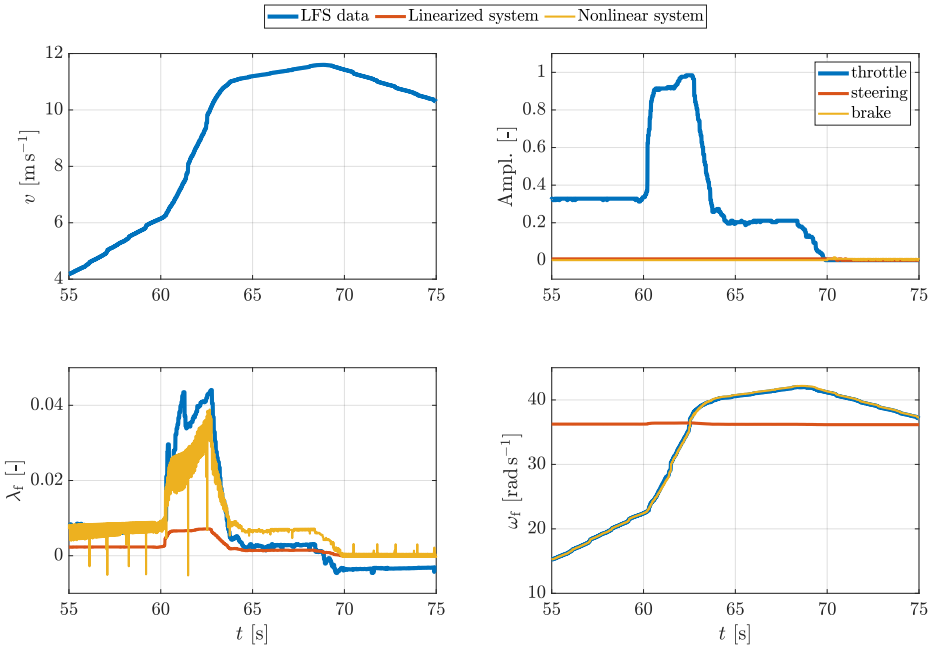

Figure 5.11: Comparison of a linearized system at constant velocity $v_{\mathrm{c}} = 10$ [m·s^{-1}], nonlinear system and the LFS simulator. λ_{f} from LFS is measured for left tire only.

A nonlinearity was added to the linearized model, to understand which part of the model affected the result. The constant speed v_{c} in Eq. 5.16 is replaced with the velocity signal from LFS (Fig. 5.12).

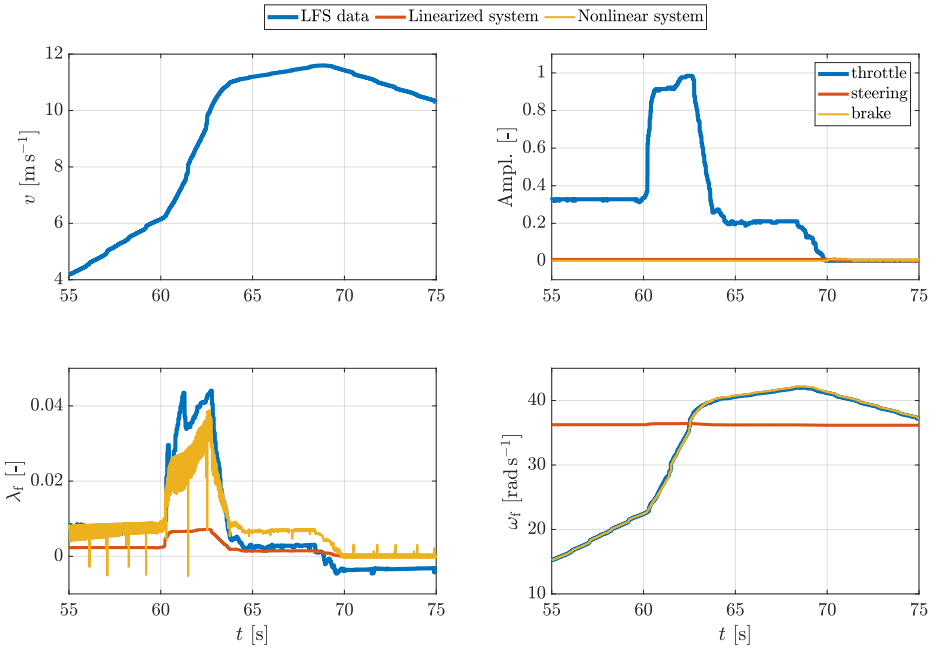

Figure 5.12: Comparison of a linearized system with added input velocity signal, nonlinear system and the LFS simulator. λ_f from LFS is measured for left tire only.

The Fig. 5.12 shows that when the speed signal is added to the linearized model, the wheels' angular velocities are almost identical. So the problem is hidden in a too rough Two-Line model approximation of the Pacejka formula (Fig. 5.8). A possible solution to this problem is to use a more complex piecewise linearization of the Pacejka formula proposed by J. Christian Gerdes' team [1]. This method will not be used, as it takes more time to create such an algorithm for the selected XF GTR car. Creating a control based on the resulting linearization does not make sense, since this model does not go beyond the DE in all tests performed.

5.5.2 Brake Input

Assuming the vice versa situation, when the braking torque is engaged and the driving torque is zero. Considering ω_f to be always positive, the linearization is similar to the one described in Eq. 5.13. The system with affine term is:

$$\begin{aligned} \dot{\omega}_f &= A_b \omega_f + B_b p_b + d_b, \\ A_b &= \left(-\frac{p^2 c_{xf}}{I_w v_c} \right), \\ B_b &= \left(-\frac{2 b_b b_s}{I_w} \right), \\ d_b &= \left(\frac{p c_{xf}}{I_w} - k F_{zf} \right). \end{aligned} \tag{5.17}$$

The substitution that removes affinity is:

$$\begin{aligned}
\omega_{\mathrm{b,lin}} &= \omega_{\mathrm{b}} + \frac{d_{\mathrm{b}}}{A_{\mathrm{b}}}, \\
\dot{\omega}_{\mathrm{b,lin}} &= \dot{\omega}_{\mathrm{b}}, \\
\lambda_{\mathrm{f}} &= \frac{p}{v_{\mathrm{c}}}\omega_{\mathrm{f}} - 1 = C_{\mathrm{b}}\omega_{\mathrm{b,lin}} + e_{\mathrm{b}}, \\
C_{\mathrm{b}} &= \frac{p}{v_{\mathrm{c}}}, \\
e_{\mathrm{b}} &= \left(-\frac{pd_{\mathrm{b}}}{Av_{\mathrm{c}}} - 1\right).
\end{aligned} \tag{5.18}$$

The resulted state-space representation is similar to Eq. 5.16:

$$\begin{aligned}
\dot{\omega}_{\mathrm{b,lin}} &= A_{\mathrm{b}}\omega_{\mathrm{b,lin}} + B_{\mathrm{b}}p_{\mathrm{b}}, \\
\lambda_{\mathrm{b,lin}} &= C_{\mathrm{b}}\omega_{\mathrm{b,lin}}
\end{aligned} \tag{5.19}$$

Creating a control based on this model is also not possible for a reason described in section 5.5.1.

6. Hierarchical Driving Envelope Protection

6.1 Lateral Envelope

When creating a hierarchy of linear systems for lateral dynamics, a problem was discovered. Fig. 6.1 shows that the zero of the system tends to go to the positive half of the real axis with increasing velocity, and after about 22 [m·s^{-1}], the car enters the oversteering state. At a speed of 30 [m·s^{-1}], the control takes ten times more time to stabilize the system, and step response begins to move in the direction opposite from the reference due to the unstable zero. When adjusting the steering wheel, such control is unacceptable. The consequences of turning the steering wheel in the opposite direction from the required one for one second can lead to severe results. A speed below 5 [m·s^{-1}] is too low to go outside the lateral envelope and not need to be controlled. In other cases, regulators were selected with the main criterion of approximately one-millisecond response time.

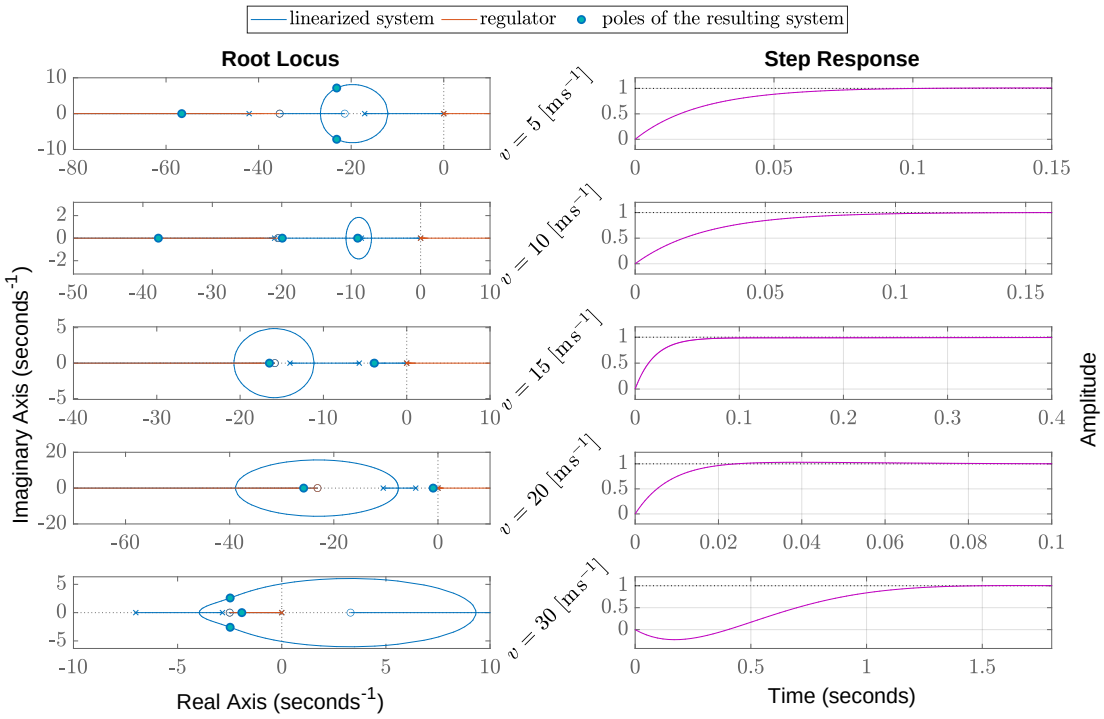

Figure 6.1: Implemented hierarchy of controllers

The previously defined lateral envelope will depend on a vehicle velocity, to give the driver more control at lower speed and more envelope protection at higher velocity (Fig. 6.2). This method is applied for both $\alpha_{\mathrm{f,max}}$ and $\alpha_{\mathrm{f,min}}$.

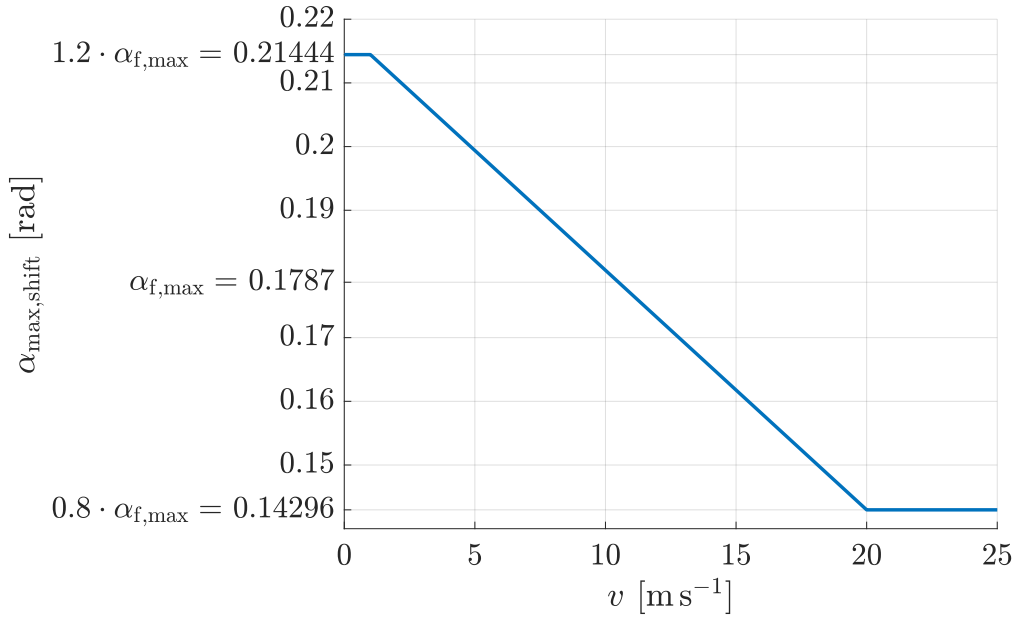

Figure 6.2: Lateral envelope shift.

The control will also be disabled for reverse and neutral gear as unnecessary. The steering angle will depend linearly on alpha to create a reference point for the controller:

$$\alpha_{\mathrm{f,ref}} = \theta \alpha_{\mathrm{max,shift}}. \tag{6.1}$$

7. Synthetic Ride Tests

7.1 Slalom

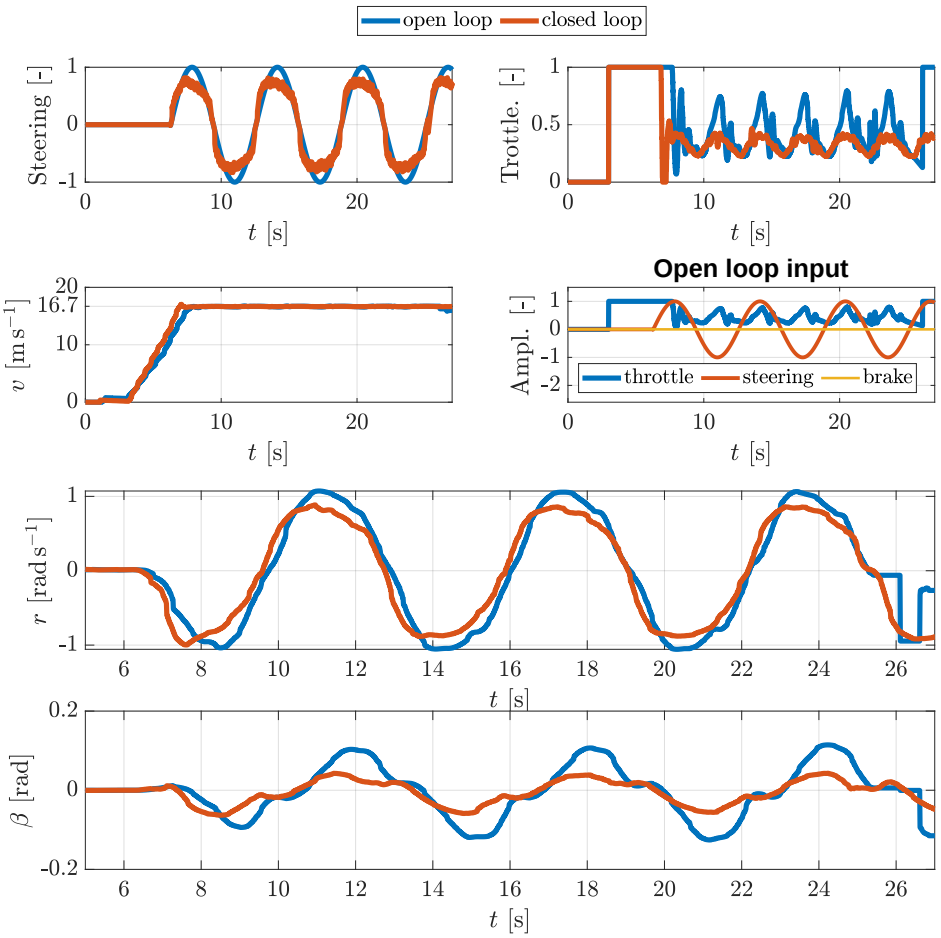

Figure 7.1: Slalom synthetic test.

The first implemented test is the slalom test. The car accelerates and maintains a constant speed of 16.7 [m·s^{-1}]. (60 [km·h^{-1}].) using simple cruise control. When this speed is reached, an input signal is sent from the steering wheel in the form of a sine wave with an amplitude equal to 1 [-] and frequency equal to 1 [rad·s^{-1}]. Fig. 7.1 - 7.2 shows that the regulator does its job and keeps the car in the lateral envelope.

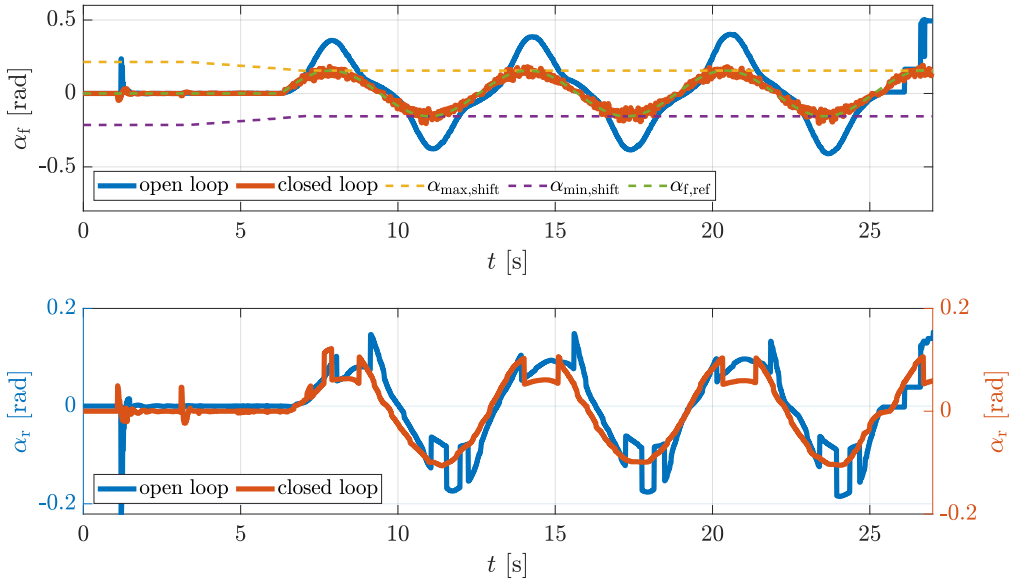

Figure 7.2: Slalom synthetic test. Slip angles comparison.

7.2 Aggressive Turn

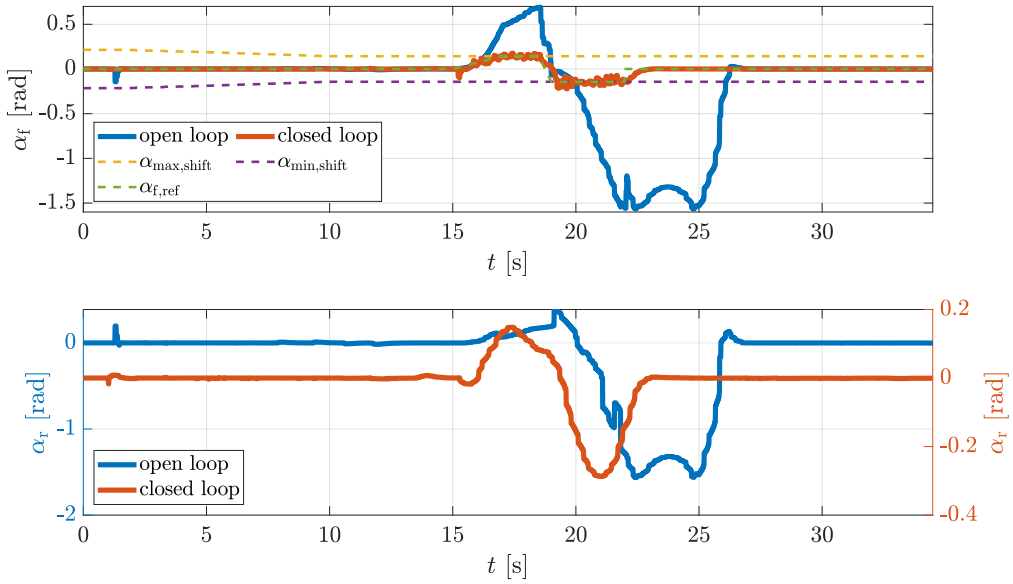

Figure 7.3: Synthesized aggressive turn test. Slip angles comparison.

The second test was performed with a constant maximum throttle and a sharp turn of the steering wheel first to one side and then to the other at 15 seconds of the test. In this test, the car without a controller skids almost to a full turn with the loss of grip. The regulator showed its ability to keep the car within the specified limits of the lateral envelope.

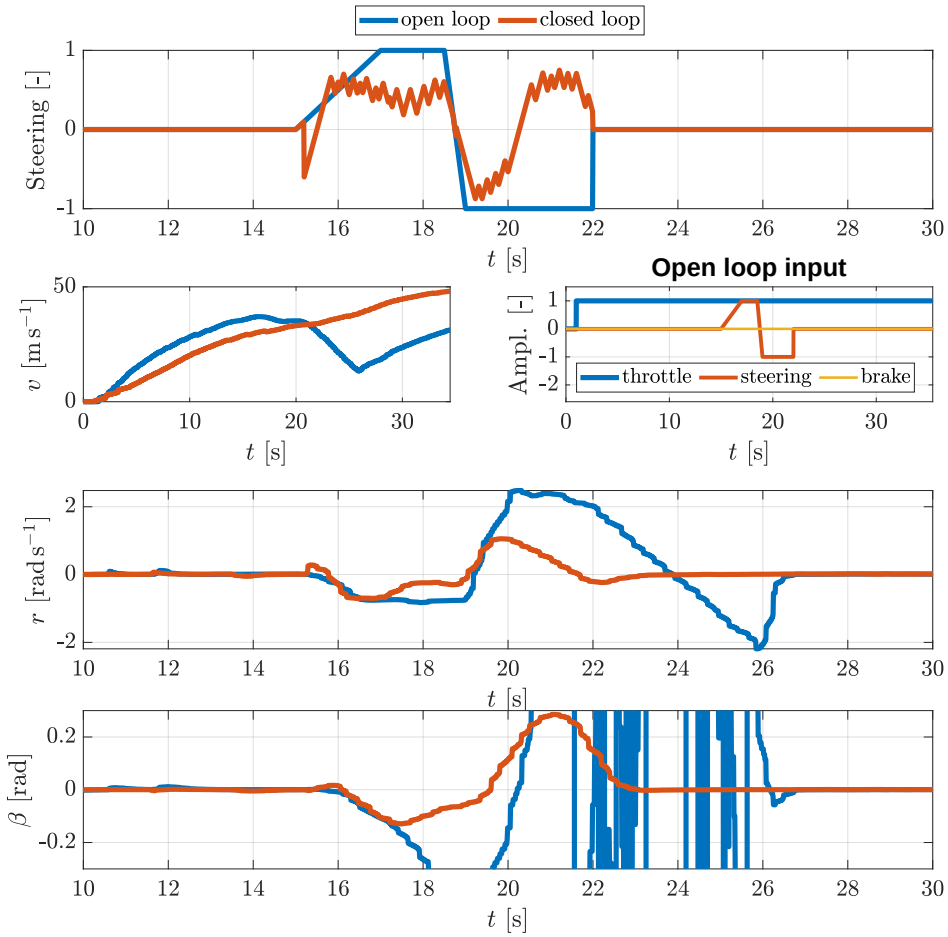

Figure 7.4: Synthesized aggressive turn test.

It is worth noting that this controller ignores the existence of the rear axle, as can be seen in both. Since the selected car is a front-wheel drive, the influence of the rear axle is not significant, but exists.

8. Real Driver Ride Tests

The track in Fig. 8.1 was selected for testing the implemented controller since it has an elaborate section with several turns in a row. There were ten reference races without the regulator's participation, as well as ten races with the control of lateral envelope enabled. A race was found in which selected section of the road took the most extended amount of time. This time (124.78 seconds) is used to measure all 20 races' average values starting from the starting point shown in Fig. 8.1. All of the data from LFS, which are displayed in the Fig. 8.2, are processed in using Eq. 8.1.

Figure 8.1: Selected track. The green line represents the starting point of the measurement. The red line is the stop point of the measurement.

Table 8.1: Race statistics.

	Average time [mins:secs:ms]	Best lap time [mins:secs:ms]
Open loop	1:45:30	1:40:52
Closed loop	1:43:71	1:41:06

Table 8.2: Average tire force utilization values for open and closed loops.

	$\overline{F_{\text{yf,util}}}[\%]$	$\overline{F_{\text{yr,util}}}[\%]$
Open loop	40.96	30.4
Closed loop	42.95	32.16

$$
\begin{aligned}
\alpha_{\mathrm{f}} &= \frac{\alpha_{\mathrm{lf}} + \alpha_{\mathrm{rf}}}{2}, \\
\alpha_{\mathrm{r}} &= \frac{\alpha_{\mathrm{lr}} + \alpha_{\mathrm{rr}}}{2}, \\
F_{\mathrm{yf,util}} &= 100 \cdot \left| \frac{F_{\mathrm{ylf}} + F_{\mathrm{yrf}}}{c_{\mathrm{D,y}} F_{\mathrm{zf}}} \right|, \\
F_{\mathrm{yr,util}} &= 100 \cdot \left| \frac{F_{\mathrm{ylr}} + F_{\mathrm{yrr}}}{c_{\mathrm{D,y}} F_{\mathrm{zr}}} \right|,
\end{aligned}
\tag{8.1}
$$

where F_{zf}, F_{zr} are from Eq. 5.8.

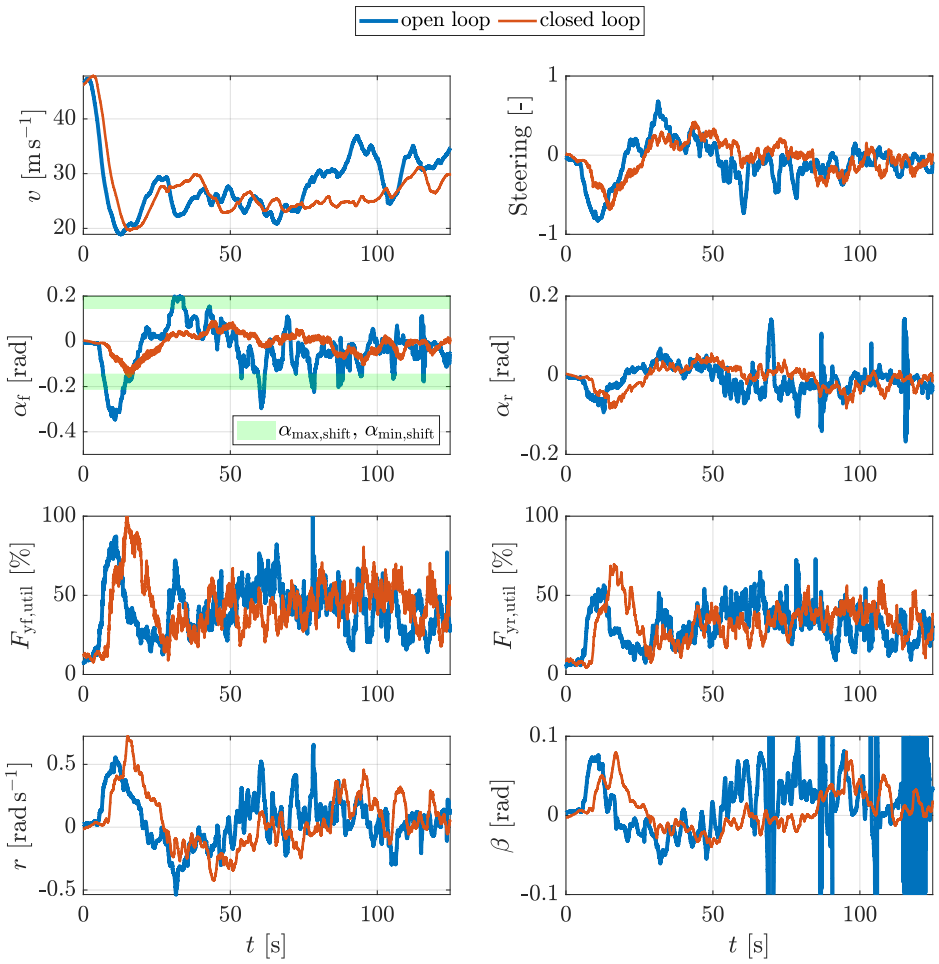

Figure 8.2: Comparison of average values on a complex road section.

Tab. 8.1 shows that when the control is enabled, there is a lateral force gain of about two percent for both car's front and rear axles, which indicates an improvement in the ability to turn. The best lap for both cases is about the same, but the controlled car's average time increased by 2 seconds (Tab. 8.1). The controller does its job entirely and holds the slip angle in the defined lateral envelope (Fig. 8.2). Although the linear model indicated oversteering dynamics with increasing speed, the real model also works perfectly at higher rates using a regulator designed for speeds up to 20 [m·s^{-1}].

9. Results

All of the goals, listed in chapter [**Objectives**] have been fully or partially achieved, namely:

- The used single-track model is described in chapter [**Used Vehicle Model**] and modified in chapter [**Single-Track Model Adaptation**].
- The driving envelope is described in chapter [**Driving Envelope Definition**].
- Lateral envelope protection was implemented using the controller hierarchy in chapter [**Hierarchical Driving Envelope Protection**].
- The control was successfully tested on the LFS simulator using synthetic tests in chapter [**Synthetic Ride Tests**].
- The control was tested and compaired in a series of races with and without control [**Real Driver Ride Tests**].

10. Conclusion

One of the main goals of this work is to create a hierarchical control of the driving envelope. When studying this topic, many difficulties were encountered, such as identifying unknown parameters, adapting a single-track model for use with an LFS simulator, describing the behavior of tires and their linearization, etc.

The created tests of car dynamics with and without the driver showed their reliability and perfectly demonstrated a controlled car's dynamics. The designed control of the lateral envelope showed excellent results and had a positive impact on the efficiency of passing a challenging track.

Unfortunately, not everything went smoothly in this work, and the chosen approximation of the tire model was not suitable for creating a hierarchical control of the longitudinal envelope. Nevertheless, the accumulated knowledge is a fundamental source for further development of more complex and advanced algorithms.

Subsequent work can use the established algorithm and improve the presented control by adding control for the rear axle and combining the influence of lateral and longitudinal on each other in the combined driving envelope, which will provide a more precise selection of the control boundaries and give even greater efficiency. Finally, the presented control method can be improved with prediction control to give a driver a smoother driving experience.

Drive-by-wire technology opens up new possibilities for driving and control a car, which I am going to investigate and improve in my future master's degree.

Bibliography

[1] Craig Earl Beal and J. Christian Gerdes. Model predictive control for vehicle stabilization at the limits of handling. *IEEE Transactions on Control Systems Technology*, 21(4):1258–1269, 2013.

[2] Denis Efremov. Unstable ground vehicles and artificial stability systems. Master's thesis, Czech Technical University in Prague, 2018.

[3] Denis Efremov. Single-track vehicle model. Available online: `https://github.com/SDS-RC-FEE-CTU-in-Prague/SingleTrack`, 2020.

[4] Denis Efremov, Tomáš Haniš, and Martin Hromčík. Introduction of driving envelope and full-time-full-authority control for vehicle stabilization systems. In *2019 22nd International Conference on Process Control (PC19)*, pages 173–178. IEEE, 2019.

[5] Denis Efremov, Martin Klaučo, Tom'aš Haniš, and Martin Hromč'ık. Driving envelope definition and envelope protection using model predictive control. In *2020 American Control Conference (ACC)*, pages 4875–4880. IEEE, 2020.

[6] Bohdan Kashel. Development of methodology for vehicle parameters' identification. B.S. thesis, Czech Technical University in Prague., 2020.

[7] LFS. Live for speed's official website. Available online: `https://www.lfs.net/`, 2020.

[8] Jiří Minarik. Yaw stabilization of 4 wheel steering cars. B.S. thesis, Czech Technical University in Prague, 2019.

[9] Martin Mondek. Active torque vectoring systems for electric drive vehicles. Master's thesis, Czech Technical University in Prague, 2018.

[10] Hans Pacejka. *Tire and vehicle dynamics*. Elsevier, 2005.

List of Figures

3.1 The vehicle coordinate system [2] . . . 5
3.2 The single-track model in the selected coordinate system [8] . . . 5
3.3 The tire coordinate system. . . . 7

4.1 DE definition for longitudinal dynamic [4]. . . . 9
4.2 DE definition for longitudinal dynamic [4] . . . 10
4.3 Combined tire force limits [4] . . . 10

5.1 Input signals for the Pacejka coefficients for lateral dynamics identification. . . . 13
5.2 Selected signals for the Pacejka coefficients for lateral dynamics identification. . . . 13
5.3 Identified Pacejka formula for lateral dynamics. . . . 14
5.4 Input signals for the Pacejka coefficients for longitudinal dynamics identification. 14
5.5 Selected output signals for the Pacejka coefficients for longitudinal dynamics identification. . . . 15
5.6 Identified Pacejka formula for longitudinal dynamics. . . . 16
5.7 Bell-shaped dependency between engine torque and engine angular velocity. . . . 17
5.8 Compirison of Pacejka and Two-Lines tire models. . . . 19
5.9 Comparison of a linearized system with the LFS simulator at constant velocity $v_c = 10$ [m·s^{-1}] . . . 19
5.10 The dependency of the transmission number on the speed of the vehicle . . . 21
5.11 Comparison of a linearized system at constant velocity $v_c = 10$ [m·s^{-1}], nonlinear system and the LFS simulator. λ_f from LFS is measured for left tire only. . . . 22
5.12 Comparison of a linearized system with added input velocity signal, nonlinear system and the LFS simulator. λ_f from LFS is measured for left tire only. . . . 23

6.1 Implemented hierarchy of controllers . . . 25
6.2 Lateral envelope shift. . . . 26

7.1 Slalom synthetic test. . . . 27
7.2 Slalom synthetic test. Slip angles comparison. . . . 28
7.3 Synthesized aggressive turn test. Slip angles comparison. . . . 28
7.4 Synthesized aggressive turn test. . . . 29

8.1 Selected track. The green line represents the starting point of the measurement. The red line is the stop point of the measurement. . . . 30
8.2 Comparison of average values on a complex road section. . . . 31

List of Tables

5.1 Inputs of the simulator 11
5.2 Used outputs of the simulator 11
5.3 Available constant parameters of the vehicle 12
5.4 Identified Pacejka coefficients for lateral dynamics. 16
5.5 Lookup table for the gear gain of the linearized system. 21

8.1 Race statistics. 30
8.2 Average tire force utilization values for open and closed loops. 30